Agricultural and Forest Meteorology 228 (2016) 120–129

Contents lists available at ScienceDirect

Agricultural and Forest Meteorology

journal homepage: www.elsevier.com/locate/agrformet

Carbon and water exchange over a temperate semi-arid shrubland during three years of contrasting precipitation and soil moisture patterns

Xin Jia[a,b,c], Tianshan Zha[a,b,*], Jinnan Gong[c], Ben Wang[a,b,c], Yuqing Zhang[a,b], Bin Wu[a,b], Shugao Qin[a,b], Heli Peltola[c]

[a] Yanchi Research Station, School of Soil and Water Conservation, Beijing Forestry University, Beijing 100083, China
[b] Key Laboratory of Soil and Water Conservation and Desertification Combating, Ministry of Education, Beijing Forestry University, Beijing 100083, China
[c] School of Forest Sciences, Faculty of Science and Forestry, University of Eastern Finland, Joensuu 80101, Finland

ARTICLE INFO

Article history:
Received 15 January 2016
Received in revised form 7 July 2016
Accepted 9 July 2016

Keywords:
Carbon balance
Carry-over
Eddy-covariance
Inter-annual variability
Soil water availability
Water use efficiency

ABSTRACT

Water is considered a key factor affecting ecosystem carbon exchange in dryland regions. However, the relationship between inter-annual variations in precipitation and ecosystem productivity remains to be clarified for arid and semi-arid areas. Based on eddy-covariance measurements, we examined how ecosystem production in a shrubland of northern China varied over three years (2012–2014) with contrasting precipitation and soil moisture patterns. Net ecosystem production (*NEP*) was 77 ± 10 ($\pm$ standard deviation), -4 ± 10 and -22 ± 5 g C m^{-2} in 2012–2014, respectively, indicating a rapid shift from an annual sink to a source of carbon. Gross ecosystem production (*GEP*), total ecosystem respiration (*TER*) and evapotranspiration (*ET*) also declined over the three years. Annual carbon and water fluxes appeared to be suppressed in years with low spring soil moisture, which declined dramatically from 2012 to 2014. *GEP* declined more than *TER* and *ET*, leading to reduced carbon sequestration capacity and water use efficiency (*WUE* = *GEP*/*ET*). Neither annual nor growing-season precipitation could explain the year-to-year variations in carbon fluxes, whereas at our site *ET* was a better proxy for water available to ecosystem carbon exchange on an annual basis. Autumn soil moisture levels were carried over winter to the following spring, and, thus, may affect the rates of leafout, plant growth and carbon uptake in the early- to mid-growing season. Our conclusions were drawn from only three years of measurements and are therefore preliminary. Longer timeseries encompassing a wider range of precipitation and soil moisture conditions are needed to confirm or refine these conclusions. Our findings highlight the importance of precipitation timing and soil moisture carry-over in controlling ecosystem productivity. Winter warming and decreases in autumn and winter precipitation may induce spring drought and thus impair the carbon sequestration potential of shrubland and steppe ecosystems in semi-arid and arid Eurasia.

1. Introduction

Global climate models project larger climatic variability and more frequent extreme events (*e.g.*, drought, storm and heat wave) in the future (Dong et al., 2011). Increases in both the severity and frequency of drought are expected to profoundly impact ecosystem structure and functioning (Jongen et al., 2011; Biederman et al., 2016). Arid and semi-arid ecosystems play an essential role in the global carbon (C) cycle, and are highly sensitive to year-to-year climatic variations (Poulter et al., 2014; Ahlström et al., 2015). Therefore, knowledge on the key factors affecting annual ecosystem production and water use efficiency in dryland areas is crucial to the projection of global C balance under changing climate.

Previous studies showed that semi-arid grasslands and steppes have larger inter-annual variability in C exchange than forest and grassland ecosystems in mesic areas, and that semi-arid ecosystems could switch from a net C sink in wet or normal years to a C source in dry years (Aires et al., 2008; Jongen et al., 2011; Scott et al., 2015; Liu et al., 2016). Although water is considered a key factor affecting ecosystem C exchange in dryland regions, the response of ecosystem production to year-to-year fluctuations in precipitation (*PPT*) often varies among sites (Sala et al., 2012; Scott et al., 2015). Despite many findings that annual *PPT* amount is a good

* Corresponding author at: Yanchi Research Station, School of Soil and Water Conservation, Beijing Forestry University, Beijing 100083, China.
E-mail addresses: tianshanzha@bjfu.edu.cn, ts_zha@hotmail.com (T. Zha).

http://dx.doi.org/10.1016/j.agrformet.2016.07.007
0168-1923/

predictor of year-to-year variations in net primary productivity (*NPP*), net ecosystem productivity (*NEP*), or gross ecosystem production (*GEP*) (Huxman et al., 2004; Scott et al., 2015; Biederman et al., 2016), some studies showed weak or non-significant relationships between annual *PPT* and ecosystem production (Xu and Baldocchi, 2004; Gilmanov et al., 2006; Jongen et al., 2011; Sala et al., 2012). Clearly, the relationship between inter-annual variations in *PPT* and ecosystem production remains to be clarified for arid and semi-arid areas. Firstly, the seasonal pattern of *PPT* can be more important than its total amount in determining the annual C balance in semi-arid ecosystems (Jongen et al., 2011; Liu et al., 2016). Secondly, hydrologic losses through runoff and evaporation may render *PPT* amount inaccurate as a measure of water availability for eco-physiological processes (Scott et al., 2015; Biederman et al., 2016). Thirdly, carry-over effects may further complicate the responses of ecosystem production to *PPT* (Sala et al., 2012).

Water-use efficiency (*WUE*) is a critical link between C and water cycling (Niu et al., 2011). Ecosystem *WUE* tends to increase with increasing *MAP* at the regional scale (Bai et al., 2008; Xiao et al., 2013), although Huxman et al. (2004) reported an opposite trend in rain use efficiency (*RUE*) across a broader *MAP* gradient (*i.e.*, data from throughout North and South America). For a given site, there is a lack of consensus regarding the response of *WUE* to drought, with either increases (Huxman et al., 2004; Bai et al., 2008; Dong et al., 2011) or decreases (Liu et al., 2012; Scott et al., 2015) in *WUE* being observed in dry years. The organizational level considered (*e.g.*, leaf, canopy and ecosystem), the way *WUE* is computed (*e.g.*, *NPP*/*PPT*, *GEP*/*ET* or *NEP*/*ET*, where *ET* denotes evapotranspiration), or the scale of analysis (*e.g.*, seasonal, inter-annual and multi-decadal) may partially account for the inconsistent *WUE* responses to dry conditions (Bai et al., 2008; Niu et al., 2011; Scott et al., 2015). A better understanding is needed of the relationship between year-to-year variations in water availability and ecosystem *WUE*, which can help constrain predictions of coupled C and water cycling under changing climate. In addition, information on how key eco-physiological parameters (*e.g.*, maximum C uptake rate and surface conductance) respond to inter-annual variations in climatic factors can help improve the modeling of C and water cycles.

Despite the extent and potential for C sequestration of desert shrublands in Eurasia, they have been less studied than forests or grasslands (Jia et al., 2014). The arid and semi-arid regions of northern China are characterized by highly variable annual *PPT* and frequent drought periods (Liu et al., 2012). Recent studies in this region have reported diurnal and seasonal dynamics of C and water exchange over shrub-dominated ecosystems, and have revealed the importance of seasonal changes in soil moisture, vapor pressure deficit (*VPD*) and canopy characteristics in controlling C sequestration (Gao et al., 2012; Liu et al., 2012; Jia et al., 2014, 2016). However, mechanisms regulating C and water dynamics depend on the timescale considered (Bai et al., 2008; Jia et al., 2014), and inter-annual dynamics should be addressed as more multi-year datasets become available. The vast Eurasia arid and semi-arid areas are expected to undergo increases in temperature and altered *PPT* patterns (Gao et al., 2012; Liu et al., 2012). In this respect, the long-term uncertainty in regional C sequestration potential lies primarily in the sensitivity of shrublands to climate variability. Therefore, it is necessary to investigate the biophysical controls on inter-annual variations in *NEP*, *WUE* and their components in these shrubland ecosystems.

The south edge of the Mu Us Desert, an ecotone between arid and semi-arid climates in northern China, is vulnerable to anthropogenic disturbances and land use changes (Jia et al., 2014, 2016). Regional conservation practices in the past two decades have resulted in a dramatic expansion of shrubland distribution, which is considered a sign of desertification reversal (Jia et al., 2016). Jia et al. (2014, 2016) reported diel and seasonal dynamics of eddy-covariance (EC) C, water and energy fluxes in a typical shrubland of the southern Mu Us Desert, showing that the ecosystem acted as a C sink of 77 g C m^{-2} in 2012. Here we focus on how C sequestration and *WUE* vary inter-annually in the shrub-dominated ecosystem. The three years (2012–2014) reported here were characterized by contrasting seasonal patterns of *PPT* and soil moisture, offering an opportunity to examine ecosystem responses to inter-annual variations in water availability. We hypothesized that decreases in water availability, which is determined by the amount and seasonal pattern of *PPT*, reduce *GEP* more than *TER* and *ET*, leading to lowered *NEP* and ecosystem *WUE*.

2. Materials and methods

2.1. Study site

This study was conducted at the Yanchi Research Station (37°42′31″N, 107°13′37″E, 1530 m a.s.l.), Ningxia, Northwest China. The site is situated at the southern edge of the Mu Us Desert, an area of mid-temperate semi-arid continental climate. The mean annual air-temperature (1954–2004) is 8.1 °C, with mean monthly temperature ranging from −8.7 °C in January to 22.4 °C in July (Jia et al., 2014). The *MAP* of 287 mm is much lower than pan-evaporation (2024 mm). In addition, *PPT* shows large seasonal (~80% falling during June–September) and inter-annual variations (145–587 mm for the period 1954–2004) (Jia et al., 2016). The growing season (May–October) coincides with the warm and wet period. The soil is sandy with a bulk density of 1.54 ± 0.08 g cm^{-3} (mean ± SD, n = 16) in the upper 10 cm of the soil profile. The studied shrubland has a total vegetation cover of ~70%. It is dominated by a mixture of xerophytic shrub species, including *Artemisia ordosica* (35% relative cover), *Hedysarum mongolicum* (30%), *H. scoparium* and *Salix psammophila* (20%), with a minor component (15%) of grass species such as *Stipa capillata* and *Agropyron cristatum*. The shrub canopy is about 1–1.5 m tall. Shrub roots are distributed mainly in the 20–50 cm soil layer. Soil water availability depends entirely on *PPT* as the water table lies 8–10 m below the ground surface. Seasonal water deficit constrains photosynthesis, *ET* and soil respiration of the studied shrub ecosystem (Jia et al., 2014, 2016).

2.2. EC and meteorological measurements

Net ecosystem CO_2 exchange (here defined as $NEE = -NEP$) and *ET* were measured with a EC system, which consisted of a 3D sonic anemometer-thermometer (CSAT-3, Campbell Scientific Inc., USA) and a closed-path infrared gas analyzer (LI-7200, LI-COR Inc., USA), mounted on a tower at 6.2 m height. Air was drawn from an inlet 20 cm away from the center of the sonic anemometer sensor volume. The sampled air was then pumped through a tube of 1 m in length and 9 mm in diameter to the LI-7200 at a flow rate of 15 L min^{-1}. On-site maintenance and sensor calibration were performed every three months. Raw signals were recorded at 10 Hz using a data logger (LI-7550, LI-COR Inc., USA). The CO_2 and water vapor (H_2O) storage terms were not estimated due to the short-statured canopy (1–1.5 m) and low sensor height, which usually render storage terms negligible. In addition, the cumulative storage terms should get close to zero as the timescale of flux integration increases (*e.g.*, daily, seasonal and annual) (Burba, 2013).

Meteorological variables were measured with sensors installed at 6 m height on the EC tower, and included incident and reflected photosynthetically active radiation (*PAR*, PAR-LITE, Kipp and Zonen, the Netherlands), wind speed (u) and direction (034B, Met One Instruments Inc., USA), net radiation (R_n, CNR-4, Kipp & Zonen, The Netherlands), and air temperature (T_a) and relative humidity (HMP155A, Vaisala, Finland). Soil heat flux (G) was calculated as

the sum of the heat flux at 10-cm depth, measured within 10 m of the tower using five soil heat flux transducers (HFP01, Hukseflux Thermal Sensors, The Netherlands), and the rate of change in heat storage in the soil layer above the transducers. All these variables were sampled at 0.1 Hz and half-hourly values stored on a data logger (CR3000, Campbell Scientific Inc., USA). Rainfall was measured daily with a manual rain gauge from 15 May to 22 July 2012, and thereafter with a tipping-bucket rain gauge (TE525WS, Campbell Scientific Inc., USA) at a distance of ~50 m from the tower. Automated rainfall measurements were recorded by a CR200X data logger (Campbell Scientific Inc., USA). We included daily rainfall values from 1 January to 14 May 2012 measured at the nearest weather station (37°48′N, 107°23′E, 1349 m a.s.l., ~20 km from the study site) to obtain the total rainfall in 2012. Snowfall, which normally contributes little to annual *PPT* at our site, was not measured. Half-hourly soil temperature (T_s) and water content (*SWC*) were measured at four depths (0.1, 0.3, 0.7 and 1.2 m) within 10 m of the tower, with three replicate sensors (ECH_2O-5TE, Decagon Devices, USA) at each depth. Details on instrumentation and sampling procedures can be found in Jia et al. (2014, 2016).

2.3. Flux calculation, quality control and gap-filling

Raw CO_2 and H_2O records were processed using the EddyPro 4.0.0 software (LI-COR Inc., USA), through steps including spike removal, double coordinate rotation, time delay corrections, frequency response corrections, detrending (block averaging) and flux computation (Burba, 2013). The Webb-Pearman-Leuning (WPL) correction was not required because the LI-7200 outputs the CO_2 mixing ratio directly (Burba, 2013). A half-hourly flux value was rejected if missing records, removed spikes and out-of-range measurements together exceeded 10% of the total records of any variable involved in calculating the flux. Calculated half-hourly fluxes were then screened for outliers following Papale et al. (2006). CO_2 and H_2O fluxes measured during calm nights (friction velocity $u^* < 0.18\ m\ s^{-1}$) were also excluded from the analyses (Jia et al., 2014). Positive values for *NEE* and *ET* denote transfer of CO_2 and H_2O upwards to the atmosphere (*i.e.*, source). Annual energy balance closure as indicated by the slope of the relationship between turbulent energy (latent plus sensible heat) and available energy (R_n–G) varied from 74% in 2014–82% in 2012. This range falls within that (0.53–0.99 with a mean of 0.79) reported for FLUXNET sites (Wilson et al., 2002). As in most previous studies, we did not apply energy-closure adjustments to EC fluxes because of the unclear cause of energy imbalance (Wilson et al., 2002).

Instrument failure and maintenance resulted in 3%, 16% and 5% missing flux records in 2012, 2013 and 2014, respectively; while the quality control procedure discarded 26%, 21% and 26% of annual flux values for 2012–2014. Consequently, 7%, 18% and 8% daytime data needed to be gap-filled in order to estimate annual C and water budgets for the three years, compared to proportions of 52%, 56% and 56% at nighttime.

Gaps in C fluxes were filled following the procedure detailed in Jia et al. (2014). In brief, data gaps of less than 2 h were filled by linear interpolation. A light-response function accounting for photoinhibition was used to fill larger daytime (incident $PAR \geq 5\ \mu mol\ m^{-2}\ s^{-1}$) gaps (Jia et al., 2014):

$$NEE_{day} = \alpha \frac{1-\beta Q}{1+\gamma Q}(Q - Q_c) \quad (1)$$

where NEE_{day} is daytime *NEE* ($\mu mol\ C\ m^{-2}\ s^{-1}$), Q is incident *PAR* ($\mu mol\ m^{-2}\ s^{-1}$), Q_c is the light compensation point. Fit parameters α, β and γ are used for the following computations:

$$Q_m = \frac{\sqrt{(\beta+\gamma)(1+\gamma Q_c)/\beta} - 1}{\gamma} \quad (2)$$

$$NEE_{\max} = -\alpha \frac{1-\beta Q_m}{1+\gamma Q_m}(Q_m - Q_c) \quad (3)$$

$$\phi_0 = -NEE'_{day}(Q=0) = -\alpha[1 + (\gamma+\beta)Q_c] \quad (4)$$

$$R_d = NEE_{day}(Q=0) = -\alpha Q_c \quad (5)$$

In Eqs. (2)–(5), Q_m is the value of Q at the most negative NEE_{day} (NEE_{max}, $\mu mol\ C\ m^{-2}\ s^{-1}$), ϕ_0 is the initial quantum yield (*i.e.*, at $Q = 0$, $mol\ C\ mol^{-1}$ photons), R_d is the average daytime ecosystem respiration rate ($\mu mol\ C\ m^{-2}\ s^{-1}$). Seasonal variation in parameter values was taken into account by fitting Eq. (1) to consecutive windows of 500 non-missing daytime data points. To estimate missing nighttime *NEE* values (NEE_{night}), we fit the Q_{10} function to the relationship between half-hourly NEE_{night} and soil temperature at 10-cm depth (T_{s_10}) for each year. Fit parameters were also used to estimate growing-season daytime *TER*. Although by bin-averaging we found that NEE_{night} plateaued or slightly reduced when T_{s_10} was greater than 20 °C (Fig. 5), the application of a sigmoidal fit instead of the Q_{10} function to half-hourly values only led to minor changes ($<8\ g\ m^{-2}$) in annually-integrated C fluxes and did not alter any of our conclusions. Missing values in the independent variables (*PAR* and T_{s_10}) of these functions were estimated using either the mean diurnal variation (MDV) method (Falge et al., 2001) or empirical relationships with other micro-meteorological measurements (*e.g.*, global solar radiation and T_a). *TER* during the non-growing season was considered equal to *NEE*. *GEP* was then estimated as *TER*–*NEE*.

Gaps in H_2O fluxes were filled following a similar procedure to that described by Amiro et al. (2006). In brief, nighttime missing values were set to zero. Daytime missing values were estimated by the regression between latent heat flux and R_n–G for good daytime data periods, based on a 240-point (half-hour period) moving window, moved in an increment of 48 points at a time. Remaining gaps in H_2O fluxes (due to missing R_n or G) were filled by applying the MDV method to consecutive 15-day windows.

2.4. Data analysis

We used the "successive days approach" together with Monte Carlo simulations to estimate the random uncertainty in annual *NEP* and *ET* (Hollinger and Richardson, 2005; Jia et al., 2014). A Monte Carlo algorithm was also used to evaluate the random uncertainty in annual *GEP* and *TER* (Hagen et al., 2006; Jia et al., 2014). The random uncertainties we evaluated (*i.e.*, the standard deviation of 2000 annual values derived from Monte Carlo simulations) only represent a partial measure of the total uncertainty for the fluxes. Other sources of uncertainty, including systematic errors arising from the choice of the u^* threshold and the gap-filling technique, were not assessed.

We estimated the bulk surface conductance (g_s) by inverting the Penman-Monteith equation (Monteith, 1965):

$$\lambda E = \frac{\Delta(R_n - G) + \rho C_p VPD g_a}{\Delta + \gamma(1 + \frac{g_a}{g_s})} \quad (6)$$

where Δ is the rate of change of saturation vapor pressure with T_a ($kPa\ K^{-1}$), ρ the air density ($kg\ m^{-3}$), C_p the specific heat capacity of air ($J\ kg^{-1}\ K^{-1}$), γ the psychrometric constant ($kPa\ K^{-1}$), *VPD* the atmospheric vapor pressure deficit (kPa). The aerodynamic conductance (g_a) was calculated as (Monteith and Unsworth, 1990):

$$g_a = \left(\frac{u}{u^{*2}} + 6.2u^{*-0.67}\right)^{-1} \quad (7)$$

Half-hourly g_s was only calculated during days with no rain and for periods when incoming shortwave radiation exceeded $100\ W\ m^{-2}$ (Jia et al., 2016).

After Huemmrich et al. (1999) and Wilson and Meyers (2007), we calculated the tower-based normalized-difference vegetation

Table 1
Climatic factors and carbon and water fluxes for 2012–2014[a].

	Year		
	2012	2013	2014
T_a (°C)	8.7	9.8	9.5
Incident *PAR* (kmol m^{-2} yr^{-1})	11.5	11.1	10.3
VPD (kPa)	0.68	0.78	0.72
Rainfall (mm yr^{-1})	335	278	342
NEP (g C m^{-2} yr^{-1})	77 ± 10	−4 ± 10	−22 ± 5
GEP (g C m^{-2} yr^{-1})	456 ± 6	359 ± 10	258 ± 7
TER (g C m^{-2} yr^{-1})	379 ± 8	363 ± 12	280 ± 6
ET (mm yr^{-1})	282 ± 3	223 ± 3	194 ± 2
WUE (g C kg^{-1} H_2O)	1.62	1.61	1.33
IWUE (g C kg^{-1} H_2O kPa)	2.34	2.92	2.52

[a] T_a, mean air temperature over all half-hourly values for each year; *PAR*, incident photosynthetically active radiation accumulated over each year; *VPD*, mean vapor pressure deficit over all half-hourly values for each year; *NEP*, net ecosystem productivity; *GEP*, gross ecosystem productivity; *TER*, total ecosystem respiration; *ET*, annual evapotranspiration; *WUE*, water use efficiency (*GEP*/*ET*); *IWUE*, mean inherent *WUE* over daily values for the carbon uptake period (*i.e.*, daily *GEP* > 0). Uncertainties for fluxes represent ± standard deviation of 2000 annual values derived from Monte Carlo simulations (see the *Data analysis* section and also refer to Jia et al. (2014) for details).

index (*NDVI*) with incident and reflected *PAR* and global solar radiation measurements. After Beer et al. (2009), *WUE* at the ecosystem level was calculated as the ratio of *GEP* to *ET*, or as the slope of the *GEP* vs. *ET* relationship; while the inherent *WUE* (*IWUE*) was calculated as ecosystem *WUE* multiplied by the mean daytime *VPD* (*i.e.*, the ratio of *GEP*·*VPD* to *ET*), or as the slope of the (*GEP*·*VPD*) vs. *ET* relationship. The *IWUE* used here can be considered an analogue of leaf-level *IWUE* (*i.e.*, the ratio of photosynthesis rate to stomatal conductance) at the ecosystem level (Beer et al., 2009).

Regression analysis was used to fit parameters used in gap-filling and to test relationships between variables of interest. Analysis of Covariance (ANCOVA) was performed to test for significant year-to-year differences in the intercept (the main effect of year) and slope (year × *ET* interaction) of regression lines of *GEP* or (*GEP*·*VPD*) vs. *ET*. Separate lines for each year were reported where the intercept and/or slope differed significantly among years. Otherwise, a common line was fit to the pooled data. For the nonlinear relationship between *WUE* and *VPD*, a common curve for the pooled data was reported (Fig. 7a) as fit parameters for separate curves showed overlapping 95% confidence intervals (*i.e.*, non-significant differences). All statistical analyses were done using R version 3.2.1 (The R Development Core Team).

3. Results

3.1. Biophysical factors

The seasonal patterns of T_a, T_{s_10}, incident *PAR* and *VPD* were similar among the three years (Fig. 1a–c, Table 1). Daily mean T_a ranged from about −8 °C in winter to 25 °C in summer. Daily mean T_{s_10} was close to T_a in winter, but was higher than T_a during the growing season. Daily incident *PAR* had minimum values (<5 mol m^{-2} day^{-1}) on cloudy winter days and maximums (~60 mol m^{-2} day^{-1}) in summer. Reflected *PAR* peaked on days with snow cover (*e.g.*, DOY 20–30, 315–320 in 2012; DOY 37–45 in 2014). *VPD* was slightly lower in 2012 than the following two years.

In general, the period between June and September received most (~80%) of the annual rainfall; and winter and early spring were rainless (Fig. 1d). Snowfall contributed little to annual *PPT*, as indicated by transient periods of snow cover (*i.e.*, peaks in reflected *PAR*, Fig. 1b). Despite this general regime, the three years were characterized by contrasting seasonal patterns of *PPT* and *SWC* (Fig. 1d and e, Table 1). Annual rainfall was higher in 2014 (19% above *MAP*) and 2012 (17% above *MAP*) than 2013 (3% below *MAP*). Periods with little rainfall and low *SWC* were evident in the summer of 2012 (*e.g.*, DOY 225–244) and 2013 (*e.g.*, DOY 215–249). In contrast, plentiful summer rain in 2014 maintained higher *SWC* at 30-cm depth (*SWC*_30) during the mid- to late-growing-season. Significant inter-annual differences in *SWC* were also noticeable in spring. Soil thaw caused a step rise in *SWC*_30 near 1 March, followed by a gradual depletion until *SWC*_30 was recharged by the first significant rain event. Spring *SWC*_30 showed sustained high values in 2012 and sustained low values in 2014. At our site, little rain or snow occurs from late autumn to early-spring, so that early-spring *SWC*_30 following soil thaw was similar to the values from the preceding autumn (Fig. 1e). *SWC* at 10-cm depth (*SWC*_10) was more affected by small rain events and surface drying than *SWC*_30, which responded mainly to rainfall events larger than 20 mm day^{-1} (Fig. 1d and e). *SWC* at 70-cm depth (*SWC*_70) was enhanced only by four heavy rainfalls over the study period.

Clear seasonal cycles were observed for tower-based *NDVI* (Fig. 1f). Spring increases in *NDVI* occurred ~20 days earlier in 2012 and 2013 than in 2014, and the seasonal maximum of *NDVI* was higher in 2012 (0.47) and 2013 (0.47) than 2014 (0.37). Moreover, 2012 and 2013 had a mean *NDVI* of 0.38 for the C uptake period (*i.e.*, daily *GEP* > 0), compared to 0.28 in 2014. Daily g_s was low in winter and reached seasonal maximum in late-spring or early summer (Fig. 1 g). A decreasing trend was observed in both the seasonal maximum and the growing-season mean of g_s from 2012 to 2014.

3.2. Carbon and water exchange

The three years differed markedly in the seasonal and annual patterns of C and water fluxes (Fig. 2, Table 1). Daily *NEE* varied in the range −4.71 to 1.63, −2.38 to 2.13 and −2.11 to 1.51 g C m^{-2} day^{-1} in 2012–2014, respectively, where negative values indicate the strength of growing-season C sink (Fig. 2a). Decreases in the maximum daily net C uptake (*i.e.*, most negative daily *NEE*) were accompanied by a delay in its occurrence (DOY 182, 203 and 243 in 2012–2014, respectively) over the three years. Maximum daily *GEP* was 6.78 g C m^{-2} day^{-1} (DOY 182) in 2012, 4.63 g C m^{-2} day^{-1} (DOY 203) in 2013 and 3.21 g C m^{-2} day^{-1} (DOY 243) in 2014. Although the C uptake period was of similar length (DOY 115–302) across the three years, the number of C sink days (*i.e.*, daily *NEE* < 0) varied, being 131, 122 and 113 days for 2012–2014, respectively. Daily *TER* was low in winter (<0.5 g C m^{-2} day^{-1}), and had seasonal peaks of 3.26, 2.76 and 2.02 g C m^{-2} day^{-1} in 2012–2014, respectively. The timing of seasonal maximum *TER* (DOY 207–209) was similar among the three years. The shrubland was a strong C sink in 2012, almost C neutral in 2013, but switched to a weak C source in 2014 (Fig. 2b, Table 1). Both annual *GEP* and *TER* were highest in 2012 and lowest in 2014. However, annual *TER* was less variable than *GEP* among years, so that inter-annual variability in *NEP* was controlled primarily by the factors controlling *GEP*.

Daily *ET* was close to zero in winter, and increased to a seasonal maximum on around DOY 200 (Fig. 2c). Maximum *ET* was 3.4, 3.6 and 2.5 mm day^{-1} for the three years, respectively. Annual *ET* was highest in 2012 and lowest in 2014 (Table 1). The low rainfall periods in August 2013 and the spring of 2014 showed reduced *ET*. Daily *WUE* during the growing season varied between 1 and 4 g C kg^{-1} H_2O (Fig. 2d). The lack of rain in August 2013 slightly enhanced *WUE* while the spring drought in 2014 led to markedly depressed *WUE* till early August. Annual *WUE* was similar in 2012 and 2013, but declined in 2014 (Table 1). Growing-season mean *IWUE* was highest in 2013 and lowest in 2014 (Table 1).

The mean diurnal variations (for non-rainy days) showed dramatic differences in *NEE*, *ET* and g_s among years during the early- to

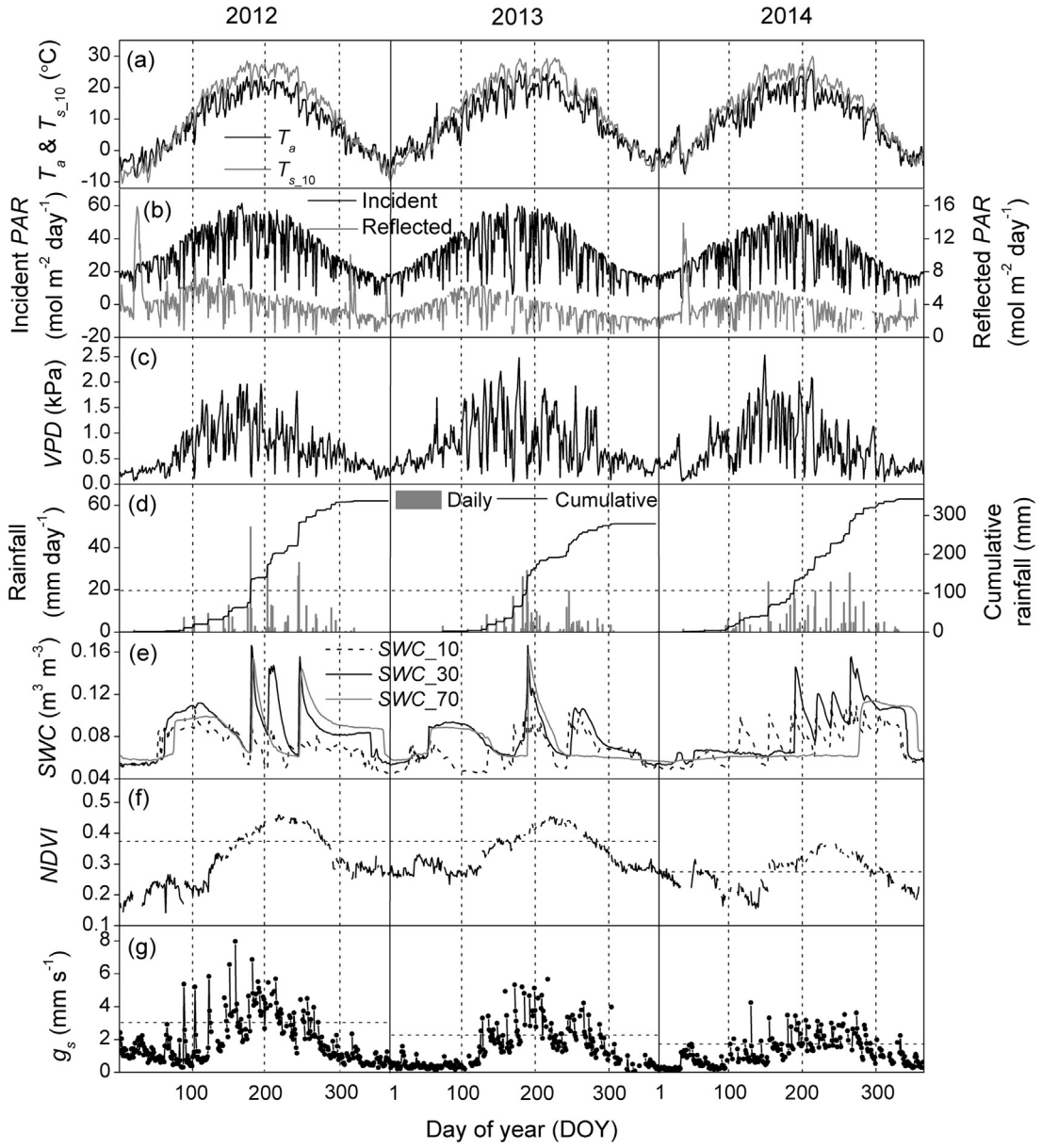

Fig. 1. Temporal variation in (a) daily mean air temperature (T_a) at 6 m above ground and soil temperature (T_{s_10}) at 10 cm depth, (b) daily-integrated incident and reflected photosynthetically active radiation (*PAR*), (c) daily mean vapor pressure deficit (*VPD*), (d) daily and cumulative rainfall, (e) soil water content (*SWC*) at three depths (10, 30 and 70 cm), (f) daily mean tower-based normalized difference vegetation index (*NDVI*) and (g) daily mean bulk surface conductance (g_s, Eq. (6)) during 2012–2014. The computations for *NDVI* and g_s were limited to half-hourly values when the incoming shortwave radiation was greater than 100 W m^{-2} and to dry surface conditions only (*i.e.*, on non-rainy days). The horizontal dashed line in (d) denotes a rain intensity of 20 mm day^{-1}; horizontal dashed lines in (f) and (g) denote mean values during the carbon uptake period (*i.e.*, daily *GEP* > 0). Climatic factors and g_s values for 2012 have been reported by Jia et al. (2014, 2016).

mid-growing season (May and July), when both daytime C uptake and nighttime C release were strongest in 2012 and lowest in 2014 (Fig. 3a and b). This pattern was also observed for daytime *ET* and g_s (Fig. 3d, e, g and h). During the late growing season (September), the diurnal courses of *NEE*, *ET* and g_s were all similar among years (Fig. 3c, f and i).

The light response curve (Eq. (1)) of NEE_{day} varied both seasonally and among years (Fig. 4). NEE_{max} (Eq. (3)) showed a unimodal seasonal pattern, peaking in July 2012, July 2013 and August–September 2014 (Fig. 4a). A delayed peak in 2014 was also found for ϕ_0 (Eq. (4), Fig. 4b). $NEE_{\max}$ in spring and summer was smaller in 2013 than 2012, and NEE_{max}, ϕ_0 and R_d (Eq. (5)) were all much lower in 2014 than the previous two years. However, all parameters converged to similar values towards the end of the growing season. NEE_{night} increased exponentially with T_{s_10} when T_{s_10} was lower than 20 °C (equivalent to a T_a of about 15 °C) (Fig. 5). NEE_{night} plateaued or declined slightly with further increases in T_{s_10}. The NEE_{night}–T_{s_10} tipping point was lower in 2014 than the other two years. Above the tipping point, NEE_{night} was highest in 2012 and lowest in 2014.

Daily *GEP* linearly increased daily *ET* (Fig. 6a), with highest slope observed in 2012 and lowest in 2014 (ANCOVA, for year, $F_{2,312} = 61.61$, $P < 0.01$; for *ET*, $F_{1,312} = 747.34$, $P < 0.01$; for year × *ET*, $F_{2,312} = 15.17$, $P < 0.01$). The slope of the relationship between (*WUE* · *VPD*) and *ET* showed a similar decreasing pattern from 2012 to 2014 (ANCOVA, for year, $F_{2,312} = 55.69$, $P < 0.01$; for *ET*, $F_{1,312} = 1408.24$, $P < 0.01$; for year × *ET*, $F_{2,312} = 7.38$, $P < 0.01$) (Fig. 6b). Bin-averaged half-hourly *WUE* decreased with increasing *VPD* (Fig. 7a). The *WUE*–*VPD* relationship was not significantly different among the three years (*i.e.*, with overlapping 95% confidence intervals for fit

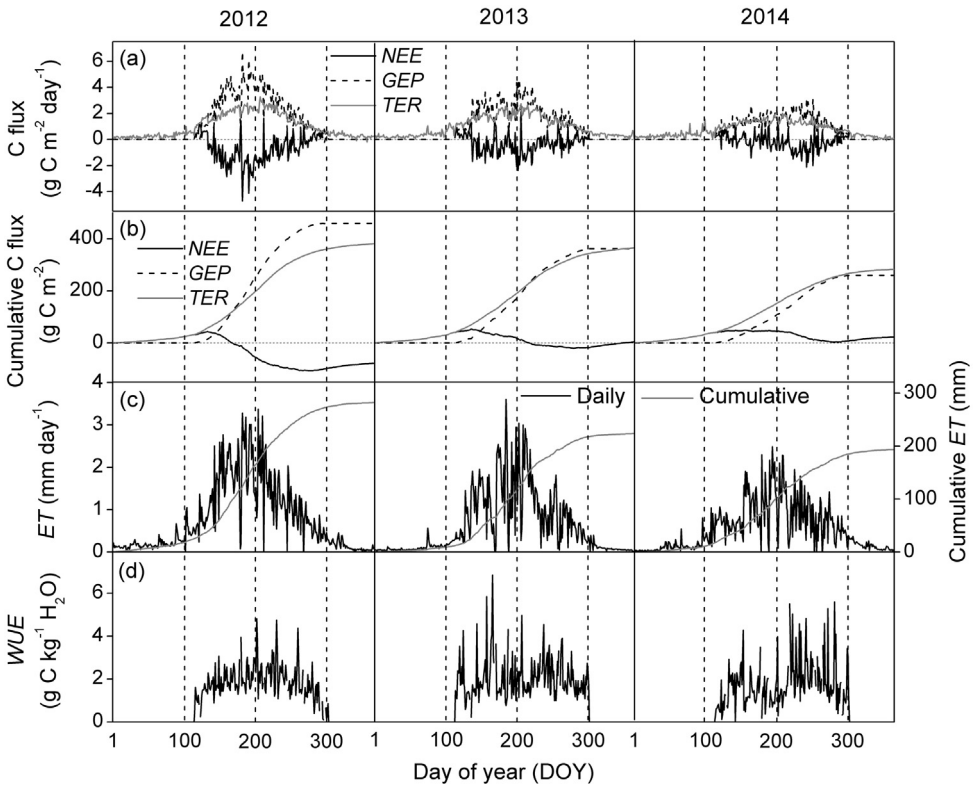

Fig. 2. Temporal variation in (a) daily carbon fluxes (*NEE*, net ecosystem CO_2 exchange; *GEP*, gross ecosystem production; *TER*, total ecosystem respiration), (b) cumulative carbon fluxes, daily and cumulative evapotranspiration (*ET*), and (d) daily ecosystem water use efficiency (*WUE*, the ratio of daily *GEP* to daily *ET*). Horizontal dotted lines in (a) and (b) represent zero reference lines. Carbon and water fluxes for 2012 have been reported by Jia et al. (2014, 2016).

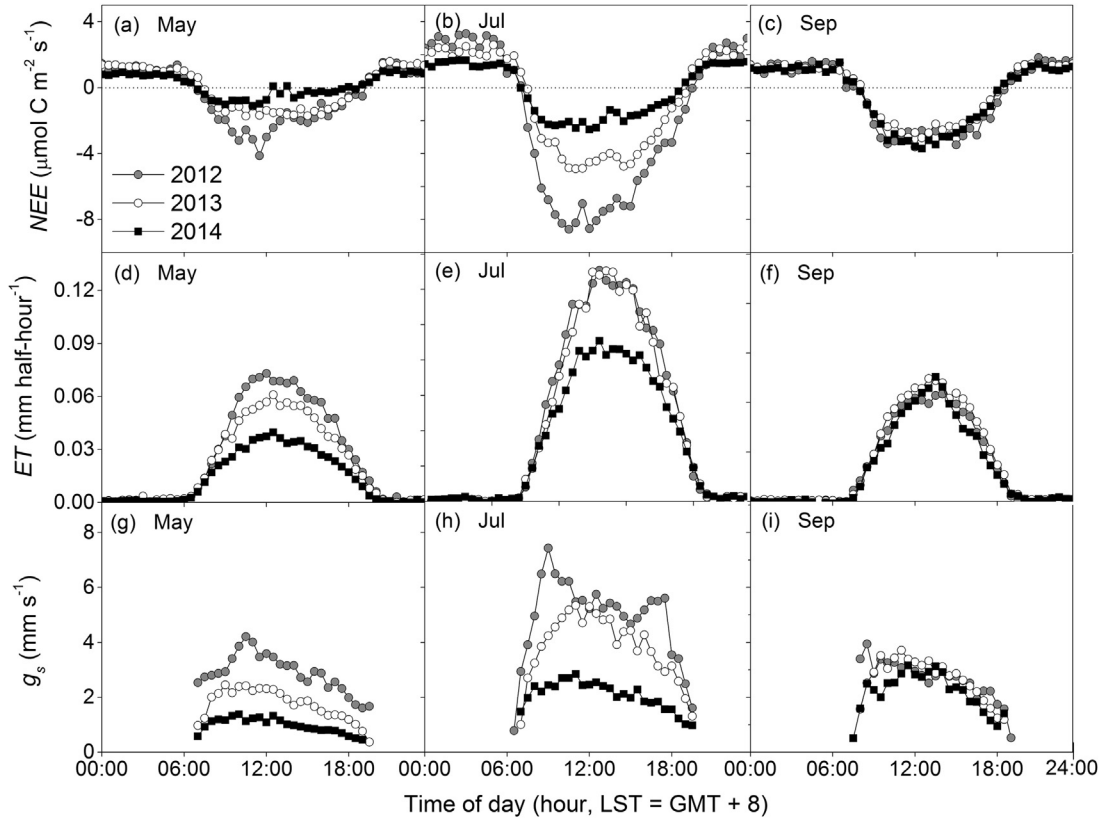

Fig. 3. Mean diurnal courses of (a) net ecosystem CO_2 exchange (*NEE*), (b) evapotranspiration (*ET*) and (c) bulk surface conductance (g_s) for May, July and September, 2012–2014. The values for g_s were based on periods when the incoming shortwave radiation was greater than 100 W m^{-2}. Horizontal dotted lines in (a–c) represent zero reference lines. Diurnal courses of *NEE* for 2012 have been reported by Jia et al. (2014).

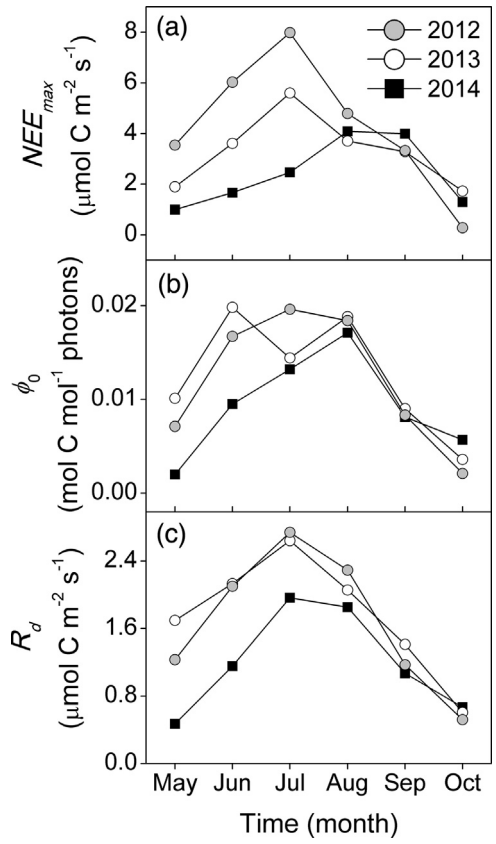

Fig. 4. Monthly parameters for the light-response curve (Eq. (1)) of daytime net ecosystem CO_2 exchange (NEE_{day}) for 2012–2014. NEE_{max}, maximum magnitude of NEE_{day} (Eq. (3)); ϕ_0, quantum yield when *PAR* equals zero (*i.e.*, absolute initial slope of the light-response curve, see Eq. (4)); R_d, average daytime ecosystem respiration rate (Eq. (5)). Monthly NEE_{max}, ϕ_0 and R_d for 2012 have been reported by Jia et al. (2014).

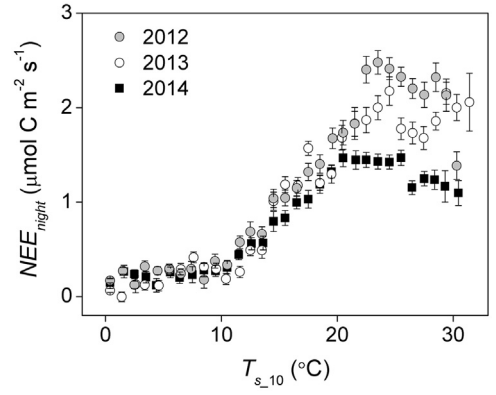

Fig. 5. Nighttime net ecosystem CO_2 exchange (NEE_{night}) as a function of soil temperature at 10 cm depth (T_{s_10}) for 2012–2014. Only data when $T_{s\_10} > 0$ °C were used. NEE_{night} was bin-averaged into 1 °C T_{s_10} intervals. Error bars indicate ±1 standard errors.

parameters) and was well described by a common exponential function. Daily *WUE* only significantly increased with *NDVI* in the growing season of 2012 ($R^2 = 0.31$, $P < 0.05$, Fig. 7b), but not in 2013 and 2014.

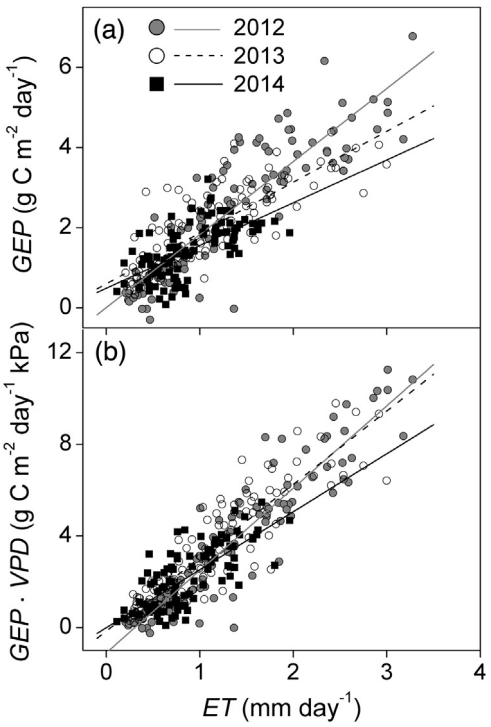

Fig. 6. Relationship between (a) daily gross ecosystem production (*GEP*) and evapotranspiration (*ET*), and between (b) daily (*GEP·VPD*) and *ET* for 2012–2014, where *VPD* is the mean daytime vapor pressure deficit. Data from rainy days as well as the subsequent two days were excluded from analysis. For (a), 2012, $y = 1.82x + 0.0086$, $R^2 = 0.78$; 2013, $y = 1.27x + 0.60$, $R^2 = 0.67$; 2014, $y = 1.07x + 0.49$, $R^2 = 0.40$. For (b), 2012, $y = 3.60x - 1.10$, $R^2 = 0.87$; 2013, $y = 3.20x - 0.15$, $R^2 = 0.82$; 2014, $y = 2.53x - 0.0016$, $R^2 = 0.56$.

4. Discussion

4.1. Does annual precipitation control ecosystem production and WUE?

PPT strongly affects the structure and functioning of semi-arid ecosystems (Huxman et al., 2004; Sala et al., 2012). Both ecosystem productivity (*NPP*, *NEP* or *GEP*) and *WUE* have been shown to vary along spatial gradients of *MAP* (Bai et al., 2008; Sala et al., 2012; Xiao et al., 2013). Annual *PPT* amount has also been identified as an important factor driving inter-annual variations in *NEP* and *WUE* for forests and grasslands (*e.g.*, Aires et al., 2008; Dong et al., 2011; Biederman et al., 2016). However, there are also some studies that found weak or non-significant relationships between annual total *PPT* and ecosystem production (Sala et al., 2012; Liu et al., 2015). More significant than annual total *PPT* is usually the seasonal pattern of *PPT* (*e.g.*, Gilmanov et al., 2006; Kwon et al., 2008; Jongen et al., 2011; Zhou et al., 2013). In the studied semi-arid shrubland, we also found that annual *PPT* could not explain year-to-year variations in ecosystem fluxes (*e.g.*, *NEP*, *GEP*, *TER*, *ET* and *WUE*) (Figs. 1 and 2, Table 1). Counterintuitively, the year with the highest rainfall (2014, 342 mm) during the study period showed the lowest ecosystem production and *WUE*.

Annual total *PPT* is not always an accurate metric of the water available to drive plant and soil CO_2 cycling (Scott et al., 2015; Biederman et al., 2016). This has been reported for arid and semi-arid ecosystems in different regions around the world (Jongen et al., 2011; Sala et al., 2012; Liu et al., 2016). Firstly, small rain events rarely recharge the soil moisture at plant rooting depth, although they may trigger increased microbial respiration in shallow soil layers (Thomey et al., 2011). Our previous studies found that roots of the dominant shrubs are mainly distributed in the 20–50 cm

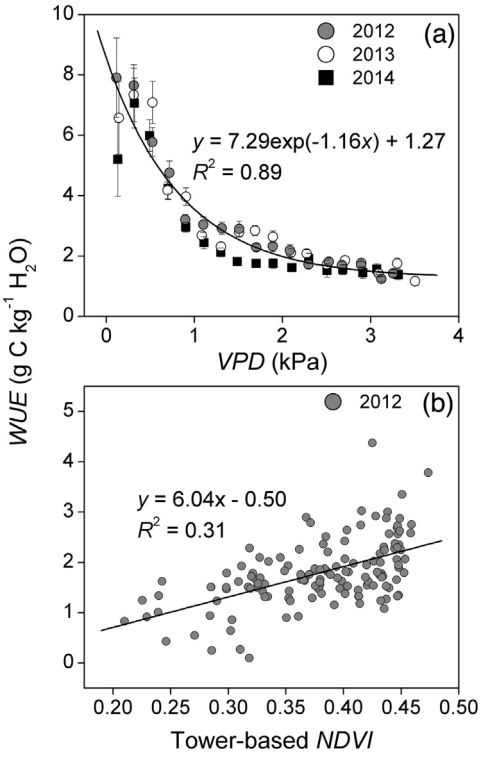

Fig. 7. (a) Relationship between ecosystem water use efficiency (*WUE*) and vapor pressure deficit (*VPD*) and for 2012–2014. To minimize the confounding effects of canopy phenology, only data for the mid-growing period (June–August) were used. Half-hourly values were bin-averaged into 0.2 kPa *VPD* increments. Error bars refer to ±1 standard error. A common curve for the pooled data is reported for the *WUE* vs. *VPD* relationship as fit parameters for separate years showed overlapping 95% confidence intervals (*i.e.*, non-significant differences). (b) Relationship between daily *WUE* and tower-based normalized difference vegetation index (*NDVI*) for 2012. The regression of *WUE* on *NDVI* was non-significant ($P > 0.05$) for 2013 and 2014.

soil layer (Wang et al., 2015), and seasonal variations in *NEE* were strongly regulated by *SWC* at 30-cm depth, rather than that at a shallower (10-cm) depth (Jia et al., 2014). The present study showed that higher annual C and water fluxes corresponded to higher spring *SWC*_30 (Figs. 1 d and 2) and that *SWC*_30 did not respond to the large number of small rainfall events (*i.e.*, <20 mm day^{-1}, Fig. 1d and e). Multiple small rain events in the spring of 2014 failed to alleviate the detrimental effects of low initial *SWC*_30 (Fig. 1d and e). It has been proposed that even for a given total annual *PPT*, different seasonal patterns, *e.g.*, frequent intermediate and small events vs. less frequent but larger events, may have contrasting effects on plant water uptake, growth and ecosystem productivity (Thomey et al., 2011).

Secondly, eco-physiological processes may depend on water availability during particular phenophases, leading to the decoupling of total *PPT* quantity and plant water demand (Dong et al., 2011; Liu et al., 2016). At our study site, low springtime soil moisture was associated with suppressed seasonal and annual ecosystem production (Figs. 1 e and 2). Ample rainfall in the summer and autumn of 2014 did not completely offset the adverse impacts of spring dry soil conditions (Figs. 1 e and 2), although late-season *NEP* and its light-response parameters had recovered to levels comparable to those in 2012 and 2013 (Figs. 3 and 4). Similarly, late *PPT* events have been found to result in smaller proportional increases in *GEP* than early events (Jongen et al., 2011; Zhou et al., 2013). A recent analysis on nine years of EC data also found that *PPT* during pre-growing season (November–April), rather than annual total or growing-season *PPT*, played an important role in controlling ecosystem productivity (Liu et al., 2016). In addition, winter to early spring *PPT* had a significant impact on the annual C balance of a Hungarian semi-arid grassland (Nagy et al., 2007).

Thirdly, hydrologic losses (*i.e.*, through runoff and evaporation) may decouple *PPT* from soil water available for biotic CO_2 exchange (Biederman et al., 2016). Recent synthesis studies on ecosystem responses to climatic variability suggest the use of *ET* as a proxy for the amount of water available to ecosystem production (Scott et al., 2015; Biederman et al., 2016). Our results support this view, showing that low productivity years were associated with low *ET*, irrespective of annual *PPT* (Figs. 1 and 2, Table 1).

4.2. Ecosystem responses to spring drought

We found that low soil moisture conditions in spring coincided with lower seasonal and annual C and water fluxes, as well as lower *WUE*, whereas a summer drought in 2013 had less impact (Figs. 1 e, 2 –4). The timing of drought plays a significant role in regulating ecosystem responses (Kwon et al., 2008; Dong et al., 2011; Zhou et al., 2013). Some previous studies in shrubland, grassland and sagebrush-steppe ecosystems also found that spring drought can be more critical to plant growth and C dynamics than summer or autumn drought (Gilmanov et al., 2006; Kwon et al., 2008; Dong et al., 2011). A severe spring drought in northern China in 2001 led to significant decreases in ecosystem *WUE*, whereas a similarly severe autumn drought in 2006 only slightly affected *WUE* (Liu et al., 2015).

Spring drought may affect ecosystem productivity through different mechanisms. Firstly, water deficit during the early growing season has been reported to hinder leaf emergence and canopy development, resulting in reduced leaf area index (*LAI*) (Aires et al., 2008; Dong et al., 2011). At our site, *NDVI* was lower in 2014 than in previous two years (Fig. 1f), likely a result of the severe spring drought in 2014 (Fig. 1e). Secondly, dry air and/or soil conditions may induce partial stomatal closure of dominant shrub species (Jia et al., 2016), as indicated by suppressed growing-season g_s (Fig. 1g), which reflects the canopy-integrated stomatal conductance. Reduced *LAI* combined with stomatal closure can lead to suppressed canopy photosynthetic capacity (Yang and Zhou, 2013; Liu et al., 2016). Thirdly, annual *GEP* has been proposed to be jointly controlled by canopy photosynthetic capacity and ecosystem-level plant phenology (Xia et al., 2015). However, the decreases in *GEP* in years with low spring soil moisture were largely attributable to suppressed canopy photosynthetic capacity (Figs. 2–4), as the C uptake period remained unchanged across years. Finally, community composition has been shown to be an important driver of ecosystem productivity in response to inter-annual variations in precipitation (Liu et al., 2016). At our site, the relative abundance of dominant species did not change much during the measurement period (unpublished data), so that shifts in community composition are not expected to account for observed patterns in C and water fluxes.

Drought events may affect *GEP* and *TER* differently, thus modifying *NEP* (Zhou et al., 2013). Our results (Figs. 1 and 2) are in line with the previous hypothesis that *GEP* is more sensitive than *TER* to spring drought in semi-arid shrublands and steppes (Kwon et al., 2008; Dong et al., 2011; Niu et al., 2011). However, short-term drought may suppress *TER* more than *GEP* because heterotrophic respiration is controlled by shallow *SWC* in the litter and upper soil layers, which dry first, whereas photosynthesis is affected by moisture that is accessible to roots in deeper soil layers (Reichstein et al., 2002; Yang and Zhou, 2013). Therefore, the interaction among the timing, severity and duration of drought should be considered when comparing the sensitivities of *GEP* and *TER* to water stress.

GEP and *ET* may also show different sensitivities to spring drought, leading to changes in *WUE*. We observed that lower annual

WUE and shallower slope of the *GEP* vs. *ET* relationship occurred in years characterized by dry spring soil conditions (Fig. 6, Table 1). Our findings are consistent with previous studies in semi-arid areas showing stronger drought impact on *GEP* than *ET* (Aires et al., 2008; Niu et al., 2011; Liu et al., 2012). It is worth mentioning that despite decreases in ecosystem-level *WUE*, leaf- and canopy-level *WUE* (*e.g.*, the ratio of assimilation to transpiration) may remain unaffected or even increase in response to water stress, as stomatal closure limits H_2O loss more than CO_2 assimilation (Dong et al., 2011; Liu et al., 2012). Therefore, the level of biological organization should be explicitly considered when modeling and interpreting *WUE* responses to drought (Niu et al., 2011). The widely reported phenological control on ecosystem *WUE* (Scott et al., 2015) was only observed in the year (*i.e.*, 2012) with high spring soil moisture (Fig. 7b), implying a more important role of air and soil moisture in regulating ecosystem *WUE* (Fig. 7a) in years with water stress.

4.3. Carry-over effects of soil moisture

PPT legacy effects (*i.e.*, effects of past *PPT* on current ecosystem properties) may simply result from the carry-over of soil moisture between years (Sala et al., 2012). At our site, little soil water recharge occurred from late autumn to early-spring, so that early-spring *SWC*_30 was similar to the values from the preceding autumn (Fig. 1e). This was also the case from the autumn of 2011 (data not shown) to the spring of 2012. Therefore, years preceded by low late-season *PPT* may undergo spring drought, negatively affecting annual ecosystem productivity and *WUE* (Fig. 2, Table 1). Our results are in line with previous findings that low winter/spring *PPT* led to inadequate recharge of deep soil moisture, and thus constrained growing-season *GEP* and *NEP* in semiarid steppe and shrubland ecosystems (Kwon et al., 2008; Liu et al., 2016). Alternatively, *PPT* legacy effects may be mediated by structural (*e.g.*, biomass, density, *LAI* and species composition) or biogeochemical (*e.g.*, litter input and nutrient availability) changes (Sala et al., 2012). Long-term studies at our site are needed to investigate how drought-induced structural and biogeochemical changes (*e.g.*, decreases in *NDVI* as a result of the severe spring drought in 2014) may influence ecosystem productivity and *WUE* in the following year.

5. Conclusions and implications

Three years of EC measurements at a semi-arid shrubland in northern China suggest the following patterns. First, inter-annual variations in water availability had large impacts on C sequestration of the shrub-dominated ecosystem, causing it to switch rapidly between an annual sink and source of CO_2. Second, spring soil moisture deficit reduced seasonal and annual *GEP* more than *TER* or *ET*, leading to decreases in C sequestration and *WUE*. Third, little soil moisture recharge occurred during winter, so that spring soil moisture following soil thaw resulted from the legacy of the preceding year's water balance. Fourth, *ET* may be a better proxy than *PPT* for water availability in order to predict C exchange on an annual basis. The observed year-to-year fluctuations in C and water fluxes were unlikely to be caused by climatic factors other than *PPT* and soil moisture, as neither temperature nor radiation showed large inter-annual variability during the measurement period. Our conclusions are preliminary and longer timeseries spanning a wider range of precipitation and soil moisture conditions are needed to confirm or refine these patterns. Our findings may apply to the vast areas of desert shrublands and steppes in northern China due to their broad climatic, edaphic and vegetation similarities.

Our findings have important implications for projecting ecosystem responses to climate change. Throughout China, the past decades have witnessed a faster rate of warming in winter than summer, a trend that is expected to continue (Piao et al., 2010). Increases in air and soil temperatures during winter can lead to shorter soil-freezing periods, higher evaporative water losses, and thus lower carry-over of soil moisture for springtime leaf emergence and expansion. Climate models predict changes in both the amount and variability of *PPT* (Thomey et al., 2011). The observed trend of decreasing autumn/winter *PPT* in northern China (Liu et al., 2005; Piao et al., 2010), even under constant or increased annual *PPT*, could intensify spring drought and thus impair the C sequestration potential of semi-arid shrubland and steppe ecosystems.

Acknowledgements

This study was funded by the Fundamental Research Funds for the Central Universities (Proj. No. 2015ZCQ-SB-02), the National Natural Science Foundation of China (NSFC, Proj. No. 31361130340, 31200537 and 31270755) and the National Basic Research Program (973 Program) of China (Proj. No. 2013CB429901). It is also related to the Finnish-Chinese research collaboration project EXTREME, between Beijing Forestry University, School of Soil and Water Conservation (team led by Prof. Tianshan Zha) and University of Eastern Finland (UEF), School of Forest Sciences (team led by Prof. Heli Peltola), funded jointly by NSFC, the Academy of Finland and UEF (Proj. No. 14921) for years 2013–2016. The U.S.–China Carbon Consortium (USCCC) supported this work via helpful discussions and the exchange of ideas. We are grateful to Dr. Alan Barr, the Associate Editor and two anonymous reviewers for providing valuable comments and suggestions on the manuscript. We also thank X. W. Yang, S. J. Liu, J. W. Mu and P. Liu for assistance with field measurements and instrument maintenance. Please contact X. Jia (xinjia@bjfu.edu.cn) or T. S. Zha (tianshanzha@bjfu.edu.cn) for accessing the data used in this study.

References

Ahlström, A., Raupach, M.R., Schurgers, G., Smith, B., Arneth, A., Jung, M., Reichstein, M., Canadell, J.G., Friedlingstein, P., Jain, A.K., Kato, E., Poulter, B., Sitch, S., Stocker, B.D., Voivy, N., Wang, Y.P., Wiltshire, A., Zaehle, S., Zeng, N., 2015. The dominant role of semi-arid ecosystems in the trend and variability of the land CO_2 sink. Science 348, 895–899.

Aires, L.M.I., Pio, C.A., Pereira, J.S., 2008. Carbon dioxide exchange above a Mediterranean C3/C4 grassland during two climatologically contrasting years. Global Change Biol. 14, 539–555.

Amiro, B.D., Barr, A.G., Black, T.A., Iwashita, H., Kljun, N., McCaughey, J.H., Morgenstern, K., Murayama, S., Nesic, Z., Orchansky, A.L., Saigusa, N., 2006. Carbon, energy and water fluxes at mature and disturbed forest sites Saskatchewan. Canada Agric. For. Meteorol. 136, 237–251.

Bai, Y., Wu, J., Xing Qi Pan, Q., Huang, J., Yang, D., Han, X., 2008. Primary production and rain use efficiency across a precipitation gradient on the Mongolian Plateau. Ecology 89, 2140–2153.

Beer, C., Ciais, P., Reichstein, M., Baldocchi, D., Law, B.E., Papale, D., Soussana, J.F., Ammann, C., Buchmann, N., Frank, D., Gianelle, D., Janssens, I.A., Knohl, A., Köstner, B., Moors, E., Roupsard, O., Verbeeck, H., Vesala, T., Williams, C.A., Wohlfahrt, G., 2009. Temporal and among-site variability of inherent water use efficiency at the ecosystem level. Global Biogeochem. Cycles 23, GB2018, http://dx.doi.org/10.1029/2008GB003233.

Biederman, J.A., Scott, R.L., Goulden, M.L., Vargas, R., Litvak, M.E., Kolb, T.S., Yepez, E.A., Oechel, W.C., Blanken, P.D., Bell, T.W., Garatuza-Payan, J., Maurer, G.E., Bore, S., Burns, S.P., 2016. Terrestrial carbon balance in a drier world: the effects of water availability in southern North America. Global Change Biol. 22, 1867–1879.

Burba, G., 2013. Eddy Covariance Method for Scientific, Industrial, Agricultural and Regulatory Applications. LI-COR Biosciences, Lincoln, USA.

Dong, G., Guo, J., Chen, J., Sun, G., Gao, S., Hu, L., Wang, Y., 2011. Effects of spring drought on carbon sequestration, evapotranspiration and water use efficiency in the Songnen Meadow Steppe in Northeast China. Ecohydrology 4, 211–224.

Falge, E., Baldocchi, D., Olson, R., Anthoni, P., Aubinet, M., Bernhofer, C., Burba, G., Ceulemans, R., Clement, R., Dolman, H., Granier, A., Gross, P., Grünwald, T., Hollinger, D., Jensen, N.O., Katul, G., Keronen, P., Kowalski, A., Lai, C.T., Law, B.E., Meyers, T., Moncrieff, J., Moors, E., Munger, J.W., Pilegaard, K., Rannik, Ü., Rebmann, C., Suyker, A., Tenhunen, J., Tu, K., Verma, S., Vesala, T., Wilson, K., Wofsy, S., 2001. Gap-filling strategies for defensive annual sums of net ecosystem exchange. Agric. For. Meteorol. 107, 43–69.

Gao, Y., Liu, L., Jia, R., Yang, H., Li, G., Wei, Y., 2012. Seasonal variation of carbon exchange from a revegetation area in a Chinese desert. Agric. For. Meteorol. 156, 134–142.
Gilmanov, T.G., Svejcar, T.J., Johnson, D.A., Angell, R.F., Saliendra, N.Z., Wylie, B.K., 2006. Long-term dynamics of production, respiration, and net CO_2 exchange in two Sagebrush-steppe ecosystems. Rangeland Ecol. Manage. 59, 585–599.
Hagen, S.C., Braswell, B.H., Linder, E., Frolking, S., Richardson, A.D., Hollinger, D.Y., 2006. Statistical uncertainty of eddy flux-based estimates of gross ecosystem carbon exchange at Howland Forest. Maine. J. Geophys. Res. 111, D08S03, http://dx.doi.org/10.1029/2005JD006154.
Hollinger, D.Y., Richardson, A.D., 2005. Uncertainty in eddy covariance measurements and its application to physiological models. Tree Physiol. 25, 873–885.
Huemmrich, K.F., Black, T.A., Jarvis, P.G., McCaughey, J.H., Hall, F.G., 1999. High temporal resolution NDVI phenology from micrometeorological radiation sensors. J. Geophys. Res 104 (D22), 27, 935–27, 944.
Huxman, T.E., Smith, M.D., Fay, P.A., Knapp, A.K., Rebecca Shaw, M., Loik, M.E., Smith, S.D., Tissue, D.T., Zak, J.C., Weltzin, J.F., Pockman, W.T., Sala, O.E., Haddad, B.M., Harte, J., Koch, G.W., Schwinning, S., Small, E.E., Williams, D.G., 2004. Convergence across biomass to a common rain-use efficiency. Nature 429, 651–654.
Jia, X., Zha, T.S., Wu, B., Zhang, Y.Q., Gong, J.N., Qin, S.G., Chen, G.P., Qian, D., Kellomäki, S., Peltola, H., 2014. Biophysical controls on net ecosystem CO_2 exchange over a semi-arid shrubland in northwest China. Biogeosciences 11, 4679–4693.
Jia, X., Zha, T., Gong, J.N., Wu, B., Zhang, Y.Q., Qin, S.G., Chen, G.P., Feng, W., Kellomäki, S., Peltola, H., 2016. Energy partitioning over a semi-arid shrubland in northern China. Hydrol. Process. 30, 972–985.
Jongen, M., Pereira, J.S., Aires, L.M.J., Pio, C.A., 2011. The effects of drought and time of precipitation on the inter-annual variation in ecosystem-atmosphere exchange in a Mediterranean grassland. Agric. For. Meteorol. 151, 595–606.
Kwon, H., Pendall, E., Ewers, B.E., Cleary, M., Naithani, K., 2008. Spring drought regulates summer net ecosystem CO_2 in a sagebrush-steppe ecosystem. Agric. For. Meteorol. 148, 381–391.
Liu, B., Xu, M., Henderson, M., Qi, Y., 2005. Observed trends of precipitation amount, frequency, and intensity in China, 1960–2000. J. Geophys. Res. 110, D08103, http://dx.doi.org/10.1029/2004JD004864.
Liu, R., Pan, L.P., Jenerette, G.D., Wang, Q.X., Cieraad, E., Li, Y., 2012. High efficiency in water use and carbon gain in a wet year for a desert halophyte community. Agric. For. Meteorol. 162–163, 127–135.
Liu, Y., Xiao, J., Ju, W., Zhou, Y., Wang, S., Wu, X., 2015. Water use efficiency of China's terrestrial ecosystems and responses to drought. Sci. Rep.-UK 5, 13799, http://dx.doi.org/10.1038/srep13799.
Liu, R., Cieraad, E., Li, Y., Ma, J., 2016. Herbaceous layer and carbon fluxes in a phreatophyte-dominated desert ecosystem. Ecosystems 19, 601–614.
Monteith, J.L., Unsworth, M.H., 1990. Principles of Environmental Physics. Butterworth-Heinemann, Oxford.
Monteith, J.L., 1965. Evaporation and environment. In: Fogg, G.E. (Ed.), The State and Movement of Water in Living Organisms. Academic Press, New York, pp. 205–234.
Nagy, Z., Pinter, K., Czóbel Sz Balogh, J., Horváth, L., Fóti Sz Barcza, Z., Weidinger, T., Csintalan Zs Dinh, N.Q., Grosz, B., Tuba, Z., 2007. The carbon budget of semi-arid grassland in a wet and a dry year in Hungary. Agr. Ecosyst. Environ. 121, 21–29.
Niu, S., Xing, X., Zhang, Z., Xia, J., Zhou, X., Song, B., Li, L., Wan, S., 2011. Water-use efficiency in response to climate change: from leaf to ecosystem in a temperate steppe. Global Change Biol. 17, 1073–1082.
Papale, D., Reichstein, M., Aubinet, M., Canfora, E., Berhofer, C., Kutsch, W., Longdoz, B., Rambal, S., Valentini, R., Vesala, T., Yakir, D., 2006. Towards a standardized processing of Net Ecosystem Exchange measured with eddy covariance technique: algorithms and uncertainty estimation. Biogeosciences 3, 571–583.
Piao, S., Ciais, P., Huang, Y., Shen, Z., Peng, S., Li, J., Zhou, L., Liu, H., Ma, Y., Ding, Y., Friedlingsteinm, P., Liu, C., Tan, K., Yu, Y., Zhang, T., Fang, J., 2010. The impacts of climate change on water resources and agricultural in China. Nature 467, 43–51.
Poulter, B., Frank, D., Ciais, P., Myneni, R.B., Andela, N., Bi, J., Beoquet, G., Canadell, J.G., Chevallier, F., Liu, Y.Y., Running, S.W., Sitch, S., van der Werf, G.R., 2014. Contribution of semi-arid ecosystems to inter-annual variability of the global carbon cycle. Nature 509, 600–603.
Reichstein, M., Tenhunen, J.D., Roupsard, O., Ourcival, J., Rambal, S., Miglietta, F., Peressotti, A., Pecchiari, M., Tirone, G., Valentini, R., 2002. Severe drought effects on ecosystem CO_2 and H_2O fluxes at three Mediterranean evergreen sites: revisions of current hypotheses? Global Change Biol. 8, 999–1017.
Sala, O.E., Gherardi, L.A., Reichmann, L., Jobbágy, E., Peters, D., 2012. Legacies of precipitation fluctuations on primary production: theory and data synthesis. Phil. Trans. R. Soc. B 367, 3135–3144.
Scott, R.L., Biederman, J.A., Hamerlynck, E.P., Barron-Gafford, G.A., 2015. The carbon balance pivot point of southwestern U.S. semiarid ecosystems: insights from the 21 st century drought. J. Geophys. Res. Biogeosci. 120, 2612–2624.
Thomey, M.L., Collins, S.L., Vargas, R., Johnson, J.E., Brown, R.F., Natvig, D.O., Friggens, M.T., 2011. Effect of precipitation variability on net primary production and soil respiration in a Chihuahuan Desert grassland. Global Change Biol. 17, 1505–1515.
Wang, B., Zha, T., Jia, X., Gong, J.N., Wu, B., Bourque, C.P.A., Zhang, Y., Qin, S.G., Chen, G.P., Peltola, H., 2015. Microtopographic variations in soil respiration and its controlling factors vary with plant phenophases in a desert-shrub ecosystem. Biogeosciences 12, 5705–5714.
Wilson, T.B., Meyers, T.P., 2007. Determining vegetation indices from solar and photosynthetically active radiation fluxes. Agric. For. Meteorol. 144, 160–179.
Wilson, K., Goldstein, A., Falge, E., Aubinet, M., Baldocchi, D., Berbigier, P., Bernhofer, C., Ceulemans, R., Dolman, H., Field, C., Grelle, A., Ibrom, A., Law, B.E., Kowalski, A., Meyers, T., Moncrieff, J., Monson, R., Oechel, W., Tenhunen, J., Valentini, R., Verma, S., 2002. Energy balance closure at FLUXNET sites. Agric. For. Meteorol. 113, 223–243.
Xia, J., Niu, S., Ciais, P., Janssens, I.A., Chen, J., Ammann, C., Afrain, A., Blanken, P.D., Cescatti, A., Bonal, D., Buchmann, N., Curtis, P.S., Chen, S., Dong, J., Flanagan, L.B., Frankenberg, C., Georgiadis, T., Gough, C.M., Hui, D., Kiely, G., Li, J., Lund, M., Magliulo, V., Marcolla, B., Merbold, L., Montagnani, L., Moors, E.J., Olesen, J.E., Piao, S., Raschi, A., Roupsard, O., Suyker, A.E., Urbaniak, M., Vaccari, F.P., Varlagin, A., Vesala, T., Wilkinson, M., Weng, E., Wohlfahrt, G., Yan, L., Luo, Y., 2015. Joint control of terrestrial gross primary productivity by plant phenology and physiology. Proc. Natl. Acad. Sci. U. S. A. 112, 2788–2793.
Xiao, J., Sun, G., Chen, J., Chen, H., Chen, S., Dong, G., Gao, S., Guo, H., Guo, J., Han, S., Kato, T., Li, Y., Lin, G., Lu, W., Ma, M., McNulty, S., Shao, C., Wang, X., Xie, X., Zhang, X., Zhang, Z., Zhao, B., Zhou, G., Zhou, J., 2013. Carbon fluxes, evapotranspiration, and water use efficiency of terrestrial ecosystems in China. Agric. For. Meteorol. 182–183, 76–90.
Xu, L., Baldocchi, D.D., 2004. Seasonal variation in carbon dioxide exchange over a Mediterranean annual grassland in California. Agric. For. Meteorol. 1232, 79–96.
Yang, F., Zhou, G., 2013. Sensitivity of temperate desert steppe carbon exchange to seasonal droughts and precipitation variations in Inner Mongolia, China. PLoS One 8, e55418, http://dx.doi.org/10.1371/journal.pone.0055418.
Zhou, J., Zhang, Z., Sun, G., Fang, X., Zha, T., McNulty, S., Chen, J., Jin, Y., Noormets, A., 2013. Response of ecosystem carbon fluxes to drought events in a poplar plantation in Northern China. For. Ecol. Manage. 300, 33–42.